Proceedings of the 3rd International Symposium on Uncertainty Quantification and Stochastic Modeling
D.A. Rade; A. M. G. Lima (Editors), ABCM, Maresias, SP, Brazil, February 15-19, 2016

Influence of additive manufacturing variability in elastic band gaps of beams with periodically distributed resonators

Danilo Beli [1] and José Roberto de França Arruda[1]

[1] Faculty of Mechanical Engineering, University of Campinas.
Rua Mendeleyev, 200. Cidade Universitária Zeferino Vaz. Campinas/SP, Brazil. CEP 13083-860.
E-mail: dbeli@fem.unicamp.br, arruda@fem.unicamp.br.

Abstract: Phononic crystals and acoustic metamaterials are periodic structures that can exhibit the elastic band gap phenomenon. The former consist of periodically varying material properties or geometry, while the latter consist of periodic boundary conditions or periodically distributed resonators. Both lead to stop bands in specific frequency intervals, where elastic waves become evanescent and, therefore, do not propagate. These structures can find applications in passive vibration and noise control. In this work, a polymer beam with periodically distributed resonators is investigated. Geometric and material variations caused by the additive manufacturing process influence the effectiveness of the band gaps, causing some skepticism about the real possibilities of fabricating metamaterials with 3D printing. Variability analysis is usually performed with sampling methods such as Monte Carlo, where a large number of analyses is necessary. Wave propagation methods such as the Spectral Element Method (SEM) are efficient for this kind of analysis. In the wave approach, only a cell needs to be computed to obtain the dispersion curves, which show the band gaps. SEM can also be used to efficiently compute the forced response of the global structure consisting of a number of quasi periodic cells. In this work some samples of a polymer beam were fabricated on a 3D printer and tested for comparison with numerical predictions. Numerical predictions and experimental results show that band gaps are reasonably robust in the presence of variability in the fabrication process. The attenuation within the band gaps decrease when compared to an exact geometry, but attenuation is still significant. Therefore, manufacturing metamaterials for vibration attenuation with 3D printers seems feasible.

Keywords: Timoshenko beam, spectral element method, acoustic metamaterial, Monte Carlo, uncertainty

NOMENCLATURE

d = substructure length, m
i = imaginary number
E=Young's modulus
f = internal force vector, N
F = nodal force vector
ln = natural logarithm
q = internal displacement vector, m
U = nodal displacement vector

Greek Symbols

Δ = cell length, m
η = structural damping ratio
λ = wavenumber, 1/m
μ = eigenvalues
σ = standard deviation
χ = mean
ψ = eigenvectors
ω = angular frequency, rad/s

Subscripts

I relative to interior DOF
g relative to global index
k relative to cell index
L relative to left DOF
R relative to right DOF

Superscripts

^ variable in the frequency domain
* non condensed matrix
^{T} matrix transpose
$^{-1}$ matrix inverse

INTRODUCTION

Periodic structures such as rails and ducts usually have a unit cell that repeats itself in one or more directions. Because of their importance, they have been studied for decades (Brillouin, 1953). Recently, new designs of periodic structures that are called phononic crystals have appeared. By reengineering phononic crystals, the concept of acoustic metamaterial emerged. The latter have aroused great interest because of their superior wave control capabilities. This control is done through elastic stop bands, which do not permit wave propagation in a specific frequency range, and pass bands, where the waves propagate. Among the applications of these new materials are vibration isolation, vibroacoustic barriers, wave tunneling and cloaking (Hussein, Leamy and Ruzzene, 2014).

While phononic crystals can be created by material and/or geometric contrast, acoustic metamaterials need a device or inclusion that works like a resonator tuned to a specific frequency range (Liu and Hussein, 2012). These resonators can be mass-spring-like systems, pillars, light and heavy inclusions, and others (Hussein and Frazier, 2013).

Physical models are important to validate concepts in the research and development stage, but also in the implementation stage, where they allow analyzing the viability of manufacturing such devices with respect to cost, time and replication (Celli and Gonella, 2015). Oftentimes, complex theoretical and numerical models are created to design structures with band gaps that are difficult to manufacture. However, additive manufacturing and its developments have enabled producing mechanical structures with complex geometry at a low cost (Hague, Campbell and Dickens, 2003).

Like any other manufacturing process, additive manufacturing also exhibit material and geometric variability, which influence the mechanical properties of the produced goods (Levy, Schindel and Kruth, 2003). In the case of phononic crystals and acoustic metamaterials, this variability affects the wave propagation within the structure. As a consequence, the band gap behavior also presents variability. One of the main points of this work is showing that the metamaterial structures manufactured with 3D printing exhibit stop bands even in the presence of variability caused by the additive manufacturing process, and that the vibration attenuation is sufficiently significant to justify their applicability.

Some researchers developed experimental studies with acoustic metamaterials, but their physical models were not fabricated by additive manufacturing. Yao *et al.* (2008) compared a theoretical mass-spring model with experimental measurements and demonstrated that the system can present a negative effective mass. Moreover, in the transmittance curves, the experimental and theoretical results are in agreement before the band gap, *i.e.*, in the acoustic mode, and in disagreement after, *i.e.*, in the optical mode. Zhu *et al.* (2011) performed numerical and experimental analyses in a periodic thin plate. They used the Finite Element Method (FEM) and reached good agreement between experimental and numerical band gaps.

Optical and acoustic modes are concepts developed in the context of condensed matter physics to describe how a crystalline structure vibrates. This definition was extend to photonic crystals and, later, to acoustic metamaterials. When the atoms in a crystal move in phase the motion behaves as a mechanical wave, while when the atoms move out of phase the motion behaves as an electromagnetic, or optical wave. Extending this concept to a structure with periodically attached resonators, in the acoustic mode the structure and the resonators vibrate in phase and in the optical mode they vibrate out of phase Pai (2010).

Analytical methods based in wave propagation, such as the Spectral Element Method (SEM) (Doyle, 1997; Lee, 2009), are largely employed in the dynamic analysis of periodic structures. In SEM, the dynamic stiffness matrix is exact within the scope of the theory used to obtain the equations of motion. Moreover, by modeling only one cell it is possible to assess free wave propagation through dispersion curves as well as the forced response in the frequency and time domains. These methods allow a reduction of the computational time, thus making them attractive for uncertainty analyses, which usually require calculating lots of different samples.

Some researchers use lumped mass-spring systems to model resonators (Liu and Hussein, 2012; Yao, Zhou and Hu, 2008). Differently, herein a continuum model based on a spectral element of a Timoshenko frame is used. This approach better describes the dynamic behavior after the band gap, *i.e.*, in the frequency range of the optical mode. Furthermore, when the wavelength is close to the cell length, a lumped system model cannot be used (Pai, 2010).

This work investigates the effect of manufacturing variability in the band gap behavior of a polymer beam with an I-shaped cross section and resonators attached periodically to it. It uses wave propagation methods and Monte Carlo sampling. Experimental results for a number of samples fabricated via 3D printing validate the numerical simulations.

In the next section, the spectral element model of the beam is presented together with a brief review of the formulation of the dispersion relation and the forced response. After that, a short introduction of the Monte Carlo method for uncertainty analysis is done. Then, the geometric model is presented, and results without and with variability are shown and discussed. Finally, the main conclusions are drawn.

THEORETICAL BACKGROUND

Dynamic analysis via SEM

The dynamic stiffness matrix (Eq. (1)) relates the forces to the displacements for a given substructure, element or unit cell in the frequency domain (Mace *et al.*, 2005). In this work, the cell, of which the geometry is presented in Fig. 1, is formed by a segment of an I-beam and two resonators, one attached to either side of the web. This matrix has degrees of freedom (DOF) called interior (I) that are not related to the left (L) or right (R) cross-section (Fig. 2).

$$\left[D^*(\omega)\right]_k\left[\hat{U}\right]_k = \begin{bmatrix} D^*_{LL} & D^*_{LI} & D^*_{LR} \\ D^*_{IL} & D^*_{II} & D^*_{IR} \\ D^*_{RL} & D^*_{RI} & D^*_{RL} \end{bmatrix}_k \begin{bmatrix} \hat{q}_L \\ \hat{q}_I \\ \hat{q}_R \end{bmatrix}_k = \begin{bmatrix} \hat{F}_L \\ \hat{F}_I \\ \hat{F}_R \end{bmatrix}_k = \left[\hat{F}\right]_k \tag{1}$$

The spectral element of a Timoshenko frame (Lee, 2009) is used to model the I-beam and the resonators. The Timoshenko frame element has two nodes and six degrees of freedom per node, three displacements and three rotations. Therefore, it includes effects of vertical bending, lateral bending, torsion and traction/compression. In the unit cell, the I-beam is composed of two elements in order to create a node in the middle, where the resonators (Fig. 2b) are placed. The dynamic stiffness of the resonators is composed by two elements, one which plays the role of the resonator spring - B_{AB}-R_{A1} and B_{AB}-R_{B1} - and the other the role of the resonator mass - R_{A1}-R_{A2} and R_{B1}-R_{B2} (Fig. 2c).

The unit cell, before the condensation process (Mace *et al.*, 2005), has six elements and seven nodes of which five are interior. By considering the cell without applied forces to the interior degrees of freedom, $[\hat{F}_I] = [0]$, the condensed dynamic stiffness matrix is obtained:

$$[D(\omega)]_k [\hat{U}]_k = \begin{bmatrix} D_{LL} & D_{LR} \\ D_{RL} & D_{RR} \end{bmatrix}_k \begin{bmatrix} \hat{U}_L \\ \hat{U}_R \end{bmatrix}_k = \begin{bmatrix} \hat{F}_L \\ \hat{F}_R \end{bmatrix}_k = [\hat{F}]_k , \quad (2)$$

where:

$$\begin{matrix} D_{LL} = D_{LL}^* - D_{LI}^* (D_{II}^*)^{-1} D_{IL}^* \\ D_{LR} = D_{LR}^* - D_{LI}^* (D_{II}^*)^{-1} D_{IR}^* \end{matrix}, \qquad \begin{matrix} D_{RL} = D_{RL}^* - D_{RI}^* (D_{II}^*)^{-1} D_{IL}^* \\ D_{RR} = D_{RR}^* - D_{RI}^* (D_{II}^*)^{-1} D_{IR}^* \end{matrix} . \quad (3)$$

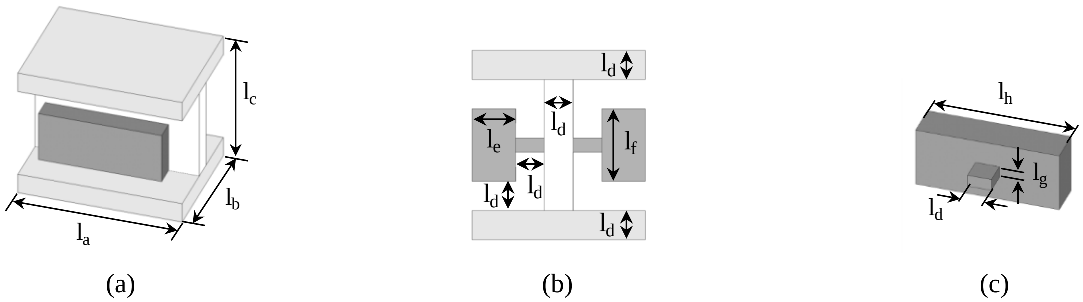

Figure 1 – Unit cell in 3D view (a), unit cell in cross-section view (b), and resonator details (c)

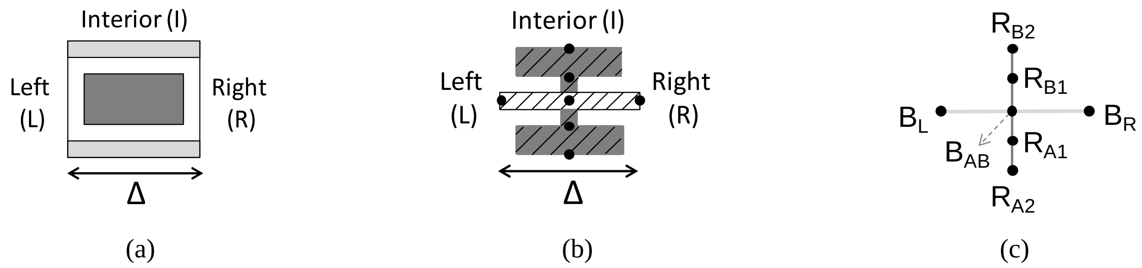

Figure 2 – Unit cell, lateral view (a), view in the neutral plane (b), and corresponding representation using 1D elements (c)

The forced response can be calculated through the global dynamic stiffness matrix, assembled as done in the finite element method. Once the boundary conditions have been applied, the corresponding displacements can be calculated as shown in Eq. (4).

$$[\hat{U}]_g = [D(\omega)]_g^{-1} [\hat{F}]_g \quad (4)$$

Alternatively, a state vector representation can be used. In this case, the transfer matrix relates the state vector of the right cross section to that of the left cross section of a unit cell (Arruda *et al.*, 2007). Considering the relation between internal and external forces of a cross section - given by Eq. (5) -, the transfer matrix (Eq. (6)) can be expressed in terms of the dynamic stiffness submatrices.

$$\begin{matrix} [\hat{f}_R]_k = [\hat{F}_R]_k \text{ and } [\hat{f}_L]_k = -[\hat{F}_L]_k \\ [\hat{q}_R]_k = [\hat{U}_R]_k \text{ and } [\hat{q}_L]_k = [\hat{U}_L]_k \end{matrix} \quad (5)$$

$$[\hat{u}_R]_k = \begin{bmatrix} \hat{q}_R \\ \hat{f}_R \end{bmatrix}_k = \begin{bmatrix} -D_{LR}^{-1} D_{LL} & D_{LR}^{-1} \\ -D_{LR} + D_{RR} D_{LR}^{-1} D_{LL} & -D_{RR} D_{LR}^{-1} \end{bmatrix}_k \begin{bmatrix} \hat{q}_L \\ \hat{f}_L \end{bmatrix}_k = [T(\omega)]_k [\hat{u}_L]_k \quad (6)$$

For periodic structures, the state vector of the right cross section of a unit cell, $[\hat{u}_R]_k^T$, can be expressed as a function of the state vector of the left cross section, $[\hat{u}_L]_k^T$, using Bloch's Theorem (Mace *et al.*, 2005):

$$[\hat{q}_R^T \quad \hat{f}_R^T]_k^T = e^{-i\lambda_k d} [\hat{q}_L^T \quad \hat{f}_L^T]_k^T \quad (7)$$

By replacing Bloch's theorem in the equation that relates the state vectors through the transfer matrix (Eq. (6)), the follow eigenproblem (Eq. (8)) is obtained:

$$[T(\omega)]_k \psi_k = \mu_k \psi_k, \quad \text{where} \quad \psi_k = \begin{bmatrix} \hat{q}_R^T & \hat{f}_R^T \end{bmatrix}_k^T \text{ and } \mu_k = e^{-i\lambda d} \tag{8}$$

This eigenproblem gives 2*n* eigenvalues and respective eigenvectors, where *n* corresponds to the number of DOF associated with each cross section. While the eigenvalues are associated to phase changing or attenuation along the beam length, the eigenvectors, or wave mode shapes, indicate the spatial distribution of the displacements and forces on the cross section. The eigenvalues and eigenvectors appear in pairs (μ_k, ψ_k^+) and $(1/\mu_k, \psi_k^-)$ that correspond to *n* waves that propagate in the forward and backward directions, respectively.

Therefore, the wavenumbers can be computed using Eq. (9).

$$\lambda_k(\omega) = \ln[\mu_k(\omega)]/(-id) \tag{9}$$

The exponential function is described numerically only between -π and π. In the computation of the natural logarithm of this function, a spatial aliasing occurs in π for the propagating part of the wavenumbers normalized by the cell length ($\lambda_k d$). This spatial aliasing is corrected in this work.

Uncertainty analysis by Monte Carlo sampling

Uncertainty analysis was performed using the deterministic model and Monte Carlo sampling. The Monte Carlo method is easy to implement, and usually employed to calibrate other uncertainty quantification methods, and it can be easily parallelized. For accurate predictions, a large number of samples is necessary, which increases the computational time (Fonseca *et al.*, 2002). One advantage of MC is the fact that it generates samples that are compatible with the statistical information about the problem, such as the spectral density, correlation, or probability density distribution.

The forced response is obtained as in the deterministic case, but the cell matrices are different because of the variability, which changes from unit cell to unit cell.

ANALYTICAL, NUMERICAL AND EXPERIMENTAL RESULTS

The model studied herein consists of an I-beam with periodic resonators attached to it. The nominal geometric dimensions of the unit cell shown in Fig. 1 are l_a = 16 mm, l_b = 12 mm, l_c = 13 mm, l_d = 2 mm, l_e = 3 mm, l_f = 5 mm, l_g = 1 mm, and l_h = 12 mm. The global structure has 21 cells and is made of polyamide, whose mean properties are shown in Table 1. The physical models with and without resonators, shown in Fig. 3, were fabricated through additive manufacturing (3D printing) using the process of selective laser sintering. The resonators are attached to both sides of the web, and the additional mass due to the resonators is around 30% of the total mass of the beam.

Table 1 – Polyamide mean properties used in the analytical and numerical models.

Property	I-beam	Resonator mass	Resonator spring
Young's modulus (GPa)	0.86	0.86	0.72
density (kg/m^3)	700	1000	700
Poisson coefficient	0.39	0,39	0,39
structural damping ratio	0.03	0.03	0.03

(a)

(b)

Figure 3 – Pictures of the physical beam model without (a) and with (b) resonators

FE models were built using BEAM188 and SOLID45 elements in Ansys®. They were used to validate the analytical model (SEM) that was employed in the uncertainty analysis, as the latter saves computational time while predicting accurate dynamic responses. Also, from the FE models built in Ansys®, the correction factor of the cross sections, the torsion constants, polar moments of inertia, and area moments of inertia which are necessary in the Timoshenko frame model were obtained.

The results in the following subsection present the dispersion relations and the forced responses for the beams with nominal values of material and geometry, *i.e.*, without variability. In the dispersion relation, the SEM results are shown. In the forced response, the wave propagation method and FE results are compared with experimental results. The experiment was performed using an impact hammer with a piezoelectric force transducer, an accelerometer, and a LMS/Scadas data acquisition system. The beam was suspended with thin nylon strings to simulate the free-free condition. The impact excitation was produced at one end of the beam and the acceleration response was measured at the opposite end.

Deterministic analysis

Results of the modal analyses of the resonator modeled with FE in Ansys® and with spectral elements are shown in Table 2. The vertical flexural mode of the resonators was tuned around to 950 Hz; moreover, the unit cell has torsional and lateral band gaps around 800 Hz and 1300 Hz, respectively. The SE results are in agreement with results obtained using BEAM188 FEs in Ansys® and in disagreement with results from the FE model built with SOLID45 elements.

Table 2 – Modal analysis of the resonator.

Mode	Frequency (Hz)			Mode Shape
	SE	BEAM188	SOLID45	
torsion	776.7	776.6	873.5	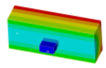
vertical flexural	941.6	941.8	970.6	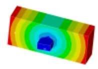
lateral flexural	1315.4	1315.6	1290.3	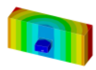

In Fig. 4, dispersion relations of cells with and without resonators are compared. The Timoshenko frame model has twelve types of waves, six forward, which are plotted in Fig. 4, and six backward, which may be related to the forward waves due to the symmetry of the unit cell. In these graphics, two of the wavenumbers correspond to vertical flexural waves, two to lateral flexural waves, one to the torsional wave, and one to the longitudinal wave.

The structural damping in the beam (modeled with a complex Young's modulus $E(1+i\eta)$) eliminates the singularity that is characteristic of the local resonance without structural damping. The resonator causes a negative derivative in the dispersion relation close to the tuned frequencies, which is consistent with the negative mass interpretation that is present in acoustic metamaterials. This range corresponds to the vibration attenuation zone (Ruzzene, 2015).

The flexural and torsional modes of the resonator create local band gaps in the torsional and in the two vertical flexural wavenumbers. Therefore, these waves have two vibration attenuation zones, a small one relative to the torsional mode and a large one relative to the flexural mode of the resonator. On the other hand, the lateral flexural mode acts in the longitudinal and in the two lateral flexural wavenumbers, which have just one local band gap. Moreover, by analyzing the evanescent and propagating behavior of the wavenumbers, the width and depth of the vibration attenuation zone can be predicted.

At lower frequencies, below local resonance, the acoustic mode dominates the response, which is characterized by an in-phase vibration of the beam and the resonators. At higher frequencies, above local resonance, the optical mode dominates, where the beam and the resonators vibrate in opposite phase. In mass-spring-like systems such as the one in this work, local resonances are created by the natural modes of the resonators, which absorb mechanical energy and do not allow the structure to vibrate in these specific frequency ranges. Therefore, within the band gap the resonators vibrate while the structure practically does not move.

For the forced response (Fig. 5), the results obtained by the analytical model (SEM), numerical model (FE), and the experimental results are in good agreement for the beam without and with resonators, but some differences appear. The band gap of the analytical model is shifted in frequency with respect to the band gap numerically predicted by SOLID45 in Ansys®. These differences, which also appear in the modal analysis of the resonator (Table 2), are due to the limitations of the simplified beam theory used in the analytical model. The beam that corresponds to the resonator spring is very short and the Timoshenko model cannot capture its complex dynamic behavior. Despite these differences, the analytical model represents fairly well the physical behavior and can be used in the variability investigation. A higher order beam model (Pagani *et al.*, 2013) could be employed to better describe the dynamic behavior of the resonators and improve the SE results; this treatment is left for future work.

The experimental results are not in perfect agreement with the analytical and numerical models in the optical mode frequency region. One possible explanation is that the manufacturing process adds uncertainties to the physical model which cause a pronounced variance in the response mainly in the optical mode region.

In addition, the actual damping could not be very well represented by the structural damping in the analytical and numerical models. The damping ratio was adjusted to approximate the resonance peak magnitudes of the measured FRFs (Fig. 5). Although this parameter is also stochastic and presents a spatial dispersion, herein we consider it deterministic because it is not relevant to determine variations in the frequency band gap.

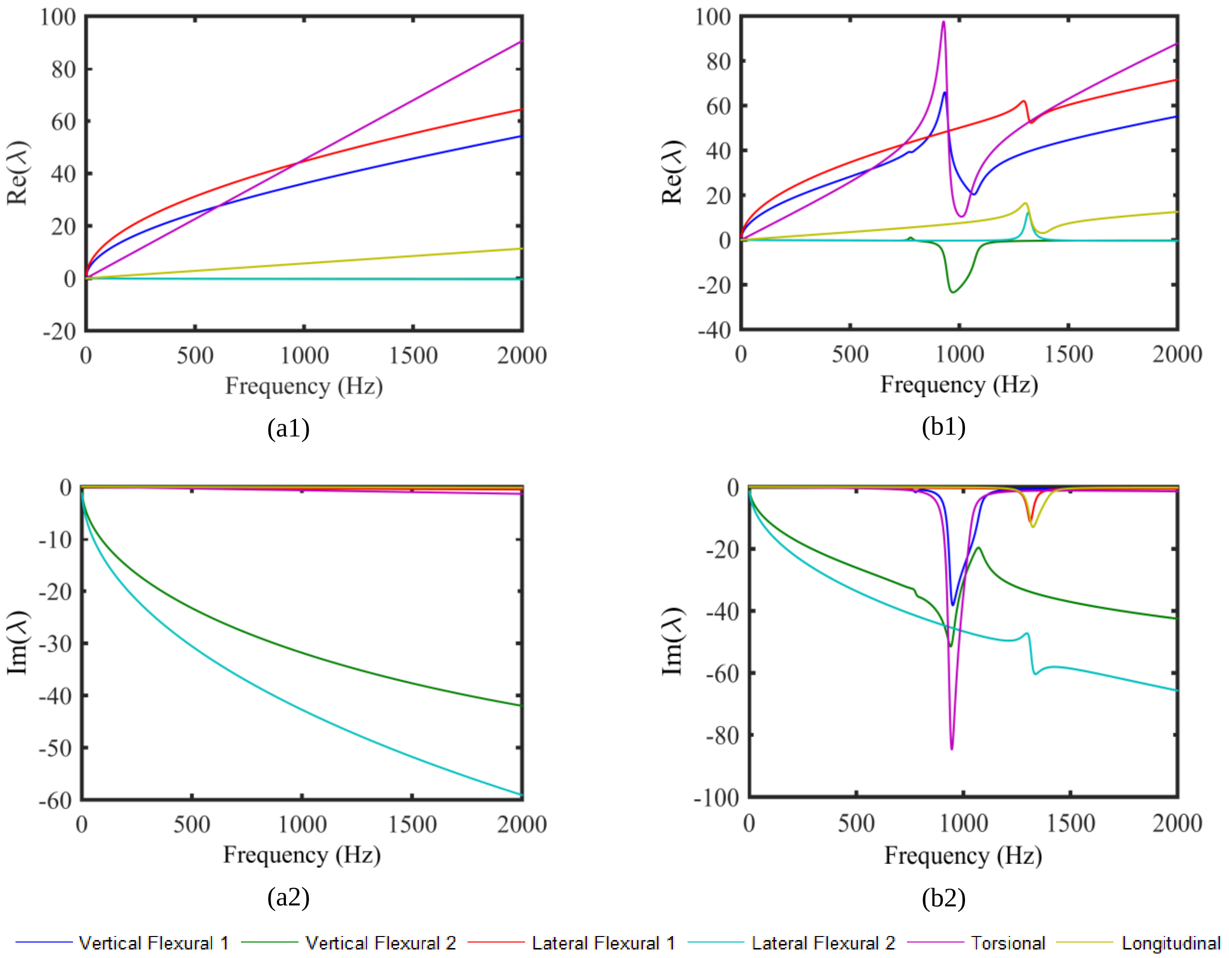

Figure 4 – Dispersion relation (SEM) for the unit cell without (a) and with (b) resonators: propagating part (1) and evanescent part (2)

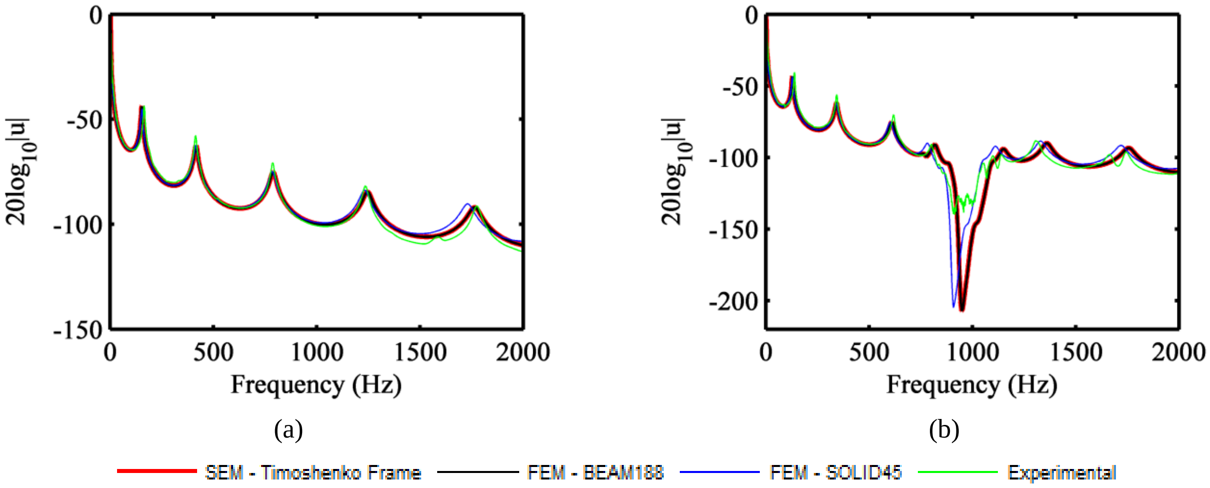

Figure 5 – Vertical forced response of the beam without (a) and with (b) resonators

Uncertainty analysis

An uncertainty analysis was performed using the Monte Carlo sampling method to better understand how the uncertainties modify the dynamic behavior of the acoustic metamaterial. Only the SE model was used, as it saves computational time and gives reasonably accurate results.

In a first approach to represent the manufacturing variability, variability in the Young's modulus and in the mass density was inserted in the SE model. First, uncertainties in the main I-beam only were considered (Fig. 6). Then, uncertainties in the resonators, which influence the band gaps (Fig. 7), were considered. The mean and the standard deviation for forced response with uncertainties were obtained. The 21 cells that compose the structure are different from each other. Uncertainties in the Young's modulus and mass density were assumed to have a gamma distribution with mean described in Table 1 and standard deviation of 10%. The number of samples was such that a convergence within 1% in the mean and standard deviation was achieved. The random number generator of Matlab® was used to generate samples for each cell with the chosen distribution.

From Fig.6 and Fig.7, it can be observed that the uncertainties in the main I-beam produce variability in the response in the optical mode, while the uncertainties in the resonators create variability in the band gap. The former also causes a change in the band gap shape when compared to the deterministic model, but it does not modify the width and the depth of the vibration attenuation zone. The latter strongly influence the dynamic response at and near the band gap, decreasing the amplitude attenuation from nominal 100 dB to actual 45 dB, and increasing the bandwidth of the band gap from 220 Hz to 280 Hz, approximately.

For both cases, the mean converges faster than the standard deviation. In the Monte Carlo method, a larger number of uncertain parameters make the convergence slower. The former case presents 21 different main I-beam cells in the structure, *i.e.* 21 different parameters, while the latter case has 42 different resonators in the structure, *i.e.* 42 different parameters. The Monte Carlo method converged faster with uncertainties in the main I-beam (Fig.6) than with uncertainties in the resonators (Fig.7).

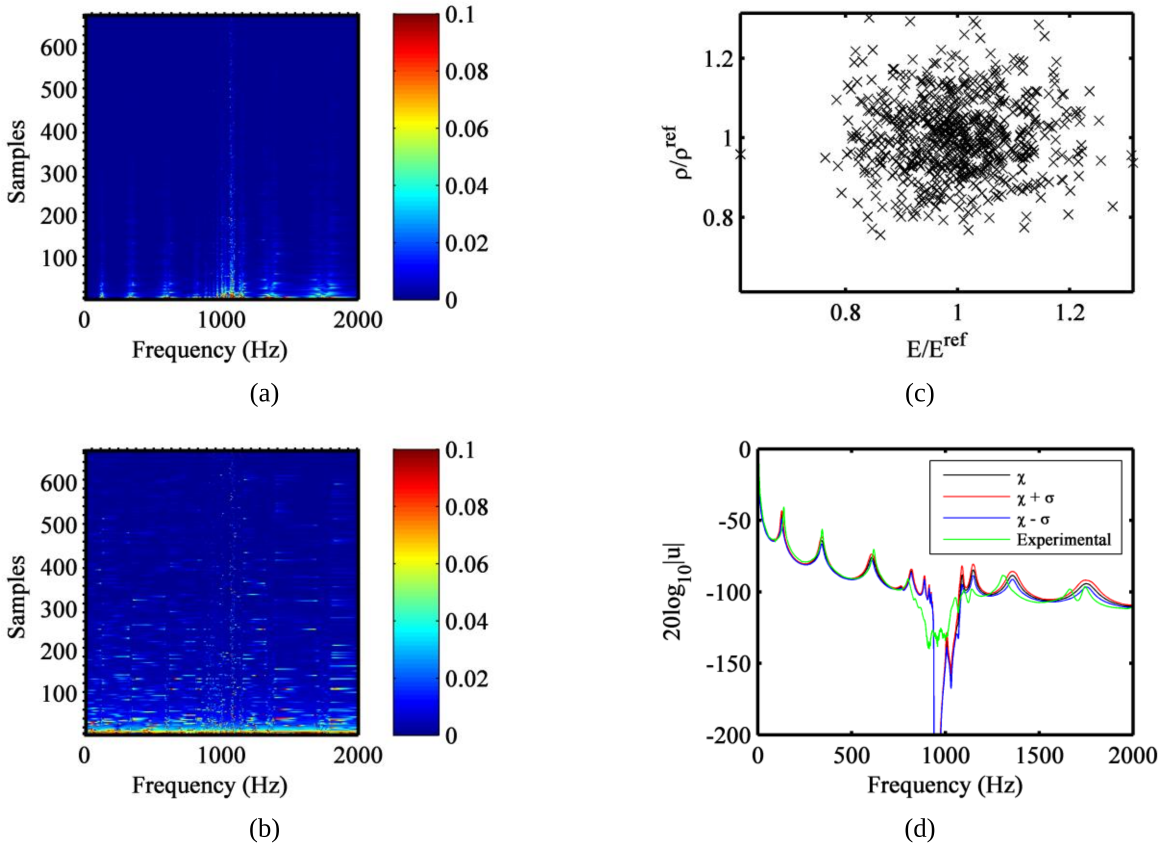

Figure 6 – Uncertainties in the main I-beam: relative error convergence map for the mean (a), for the standard deviation (b), dispersion data of one unit cell (c) and forced response (d)

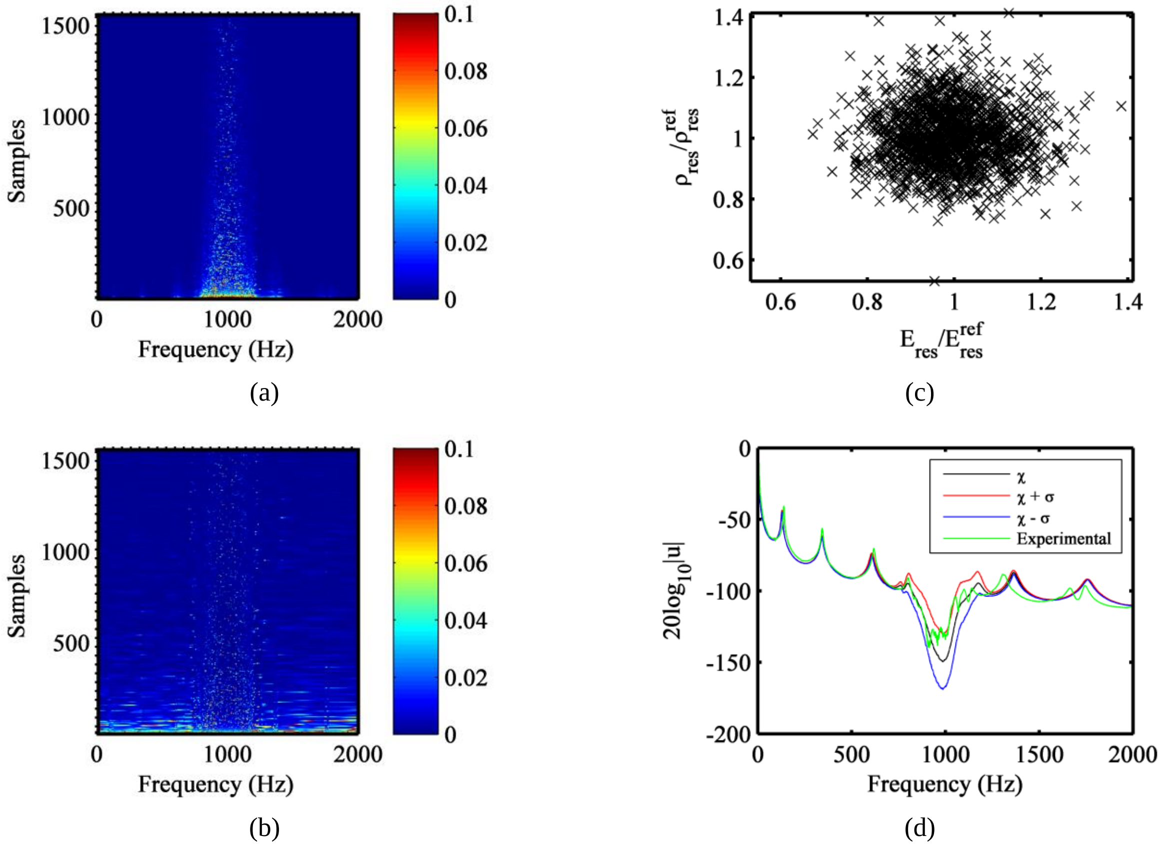

Figure 7 – Uncertainties in the resonators: relative error convergence map for the mean (a), for the standard deviation (b), dispersion data for one resonator (c) and forced response (d)

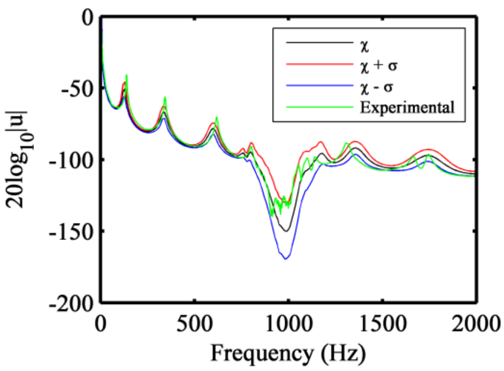

Figure 8 – Uncertainties in the main I-beam with σ = 20% and in the resonators with σ = 10%

The experimental forced responses are in good agreement with the prediction by SEM with uncertainty in the resonators. The dynamic behavior is reasonably well described in the frequency range that includes the acoustic mode and the band gap. The optical mode response is better represented with uncertainties in the main I-beam because its variability increases with frequency. Thus, SEM results with a combination of variability in both, main I-beam with σ=20% and resonators with σ=10%, represent the experimental forced response in the whole frequency range (Fig. 8) investigated.

In this work, the dispersion of material properties of different periodic cells was considered independent because the cell length (16 mm) is larger than the expected correlation length of the spatial distribution of the material properties along the beam caused by the additive manufacturing process. The assumption of independent dispersion among periodic cells seems to be consistent, as the predicted variations agreed fairly well with experimental results. Nevertheless, this topic needs further investigation.

With the presented results, it has been shown that the variability of the additive manufacturing process does not hinder the use of metamaterials for vibration attenuation. Although lessened by variability, the vibration attenuation within the band gap is still significant.

An important question is the prediction of how the band gaps behave with different variation levels. Tolerances in manufacturing processes are associated with time and cost. Therefore, predicting maximum tolerances can be help to save resources. Figure 9 shows the forced response obtained by varying the tolerance in the Young's modulus and mass density of the resonator material. It can be observed that the higher the variability the larger is the band gap width, but the shallower is the vibration attenuation. In this case a band gap is obtained for a variability of approximately 15% in the material proprieties of the resonator. Above this value, the attenuation is not guaranteed.

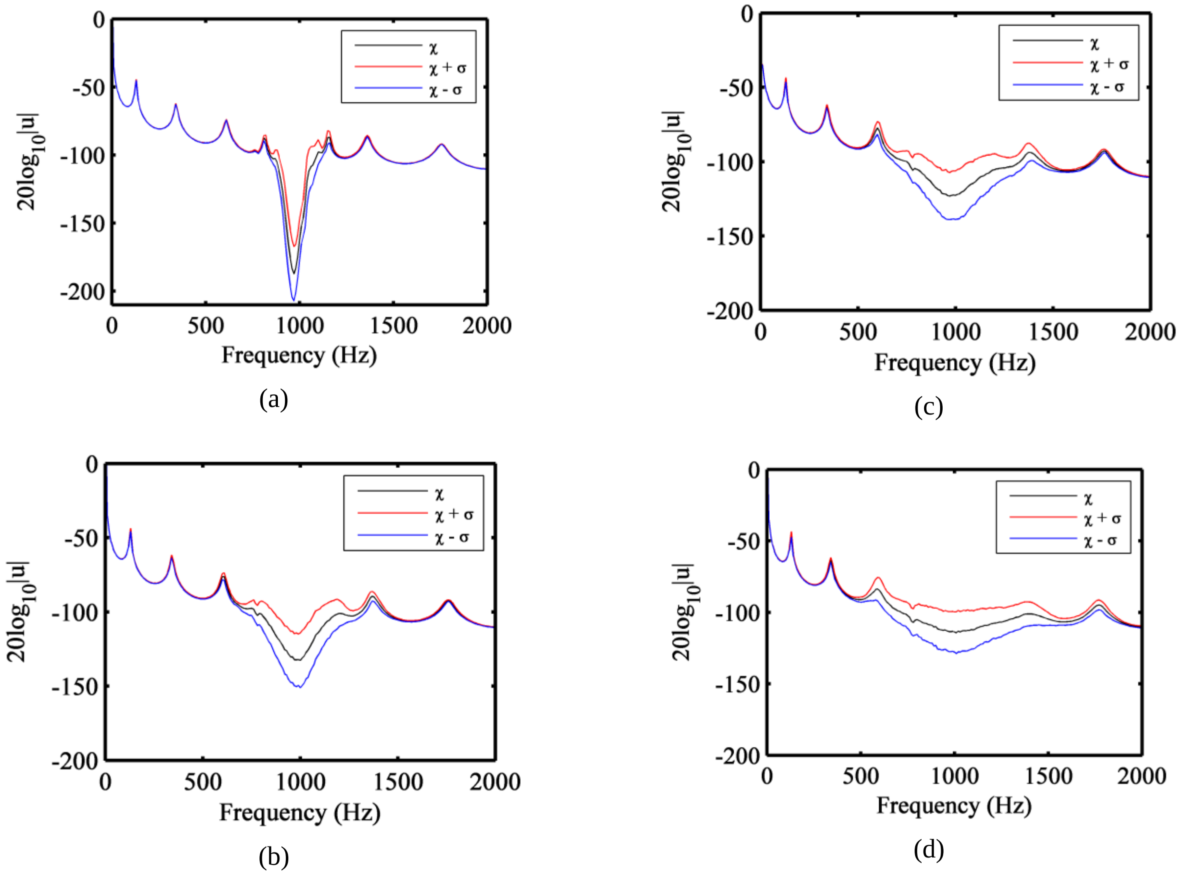

Figure 9 – Standard deviation in the resonators of 5% (a), 15% (b), 20% (c) and 30% (d)

CONCLUSIONS

In this work, dispersion relations and the forced responses for a beam with periodic resonators were computed and compared with experimental results. Differences between the analytical (wave-based) and numerical (FEM) predictions occur in the frequency range of the so-called optical mode. By considering uncertainties in the resonators and in the main I-beam, a better agreement was obtained between analytical and experimental results.

The uncertainties in the additive manufacturing process influence the forced response and decrease the depth of the band gap, but the band gap phenomenon was still observable. The band gap is wider and shallower than the deterministic one, but can still be used to attenuate vibration at desired frequencies. However, a control of the manufacturing tolerances is required to guarantee the functionality of the band gap.

ACKNOWLEDGMENTS

The authors would like to thank CTI Renato Archer for manufacturing the beam samples used in this work in their additive manufacturing facility through the ProEXP program, and also to acknowledge the financial support of CNPq and FAPESP, through project numbers 156459/2013-2 and 2014/19054-6, respectively.

REFERENCES

Arruda, J.R.F, Ahmida, K.M., Ichchou, M.N. and Mencik, J.M., 2007, "Investigating the relations between the wave finite element and spectral element methods using simple waveguides", Proceedings of 19th International Congress of Mechanical Engineering (COBEM), Brasilia, Brazil, 10p.

Brillouin, L., 1953, "Wave Propagation in Periodic Structures", Dover Phoenix Editions, New York, USA, 255p.

Celli, P. and Gonella, S., 2015, "Manipulating Waves with LEGO® Bricks: A Versatile Experimental Platform for Metamaterial Architectures", arXiv preprint arXiv:1505.04456.

Doyle, J.F., 1997, "Wave Propagation in Structures", Springer, New York, USA, 320 p.

Fonseca, J., Mares, C., Friswell, M. and Mottershead, J., 2002, "Review of Parameter Uncertainty Propagation Methods in Structural Dynamic Analysis", Proceedings of ISMA2002, Vol. IV, Leuven, Belgium, pp. 1853-1860.

Hague, R., Campbell, I. and Dickens, P., 2003, "Implications on design of rapid manufacturing", Proceedings of the Institution of Mechanical Engineers, Part C: Journal of Mechanical Engineering Science, Vol. 217, No. 1, pp. 25-30.

Hussein, M.I. and Frazier, M.J., 2013 "Metadamping: An emergent phenomenon in dissipative metamaterials", Journal of Sound and Vibration, Vol. 332, pp. 4767-4774.

Hussein, M.I., Leamy, M.J. and Ruzzene, M., 2014, "Dynamics of Phononic Materials and Structures: Historical Origins, Recent Progress, and Future Outlook", Applied Mechanics Reviews, Vol. 66, pp. 040802-1-38.

Lee, U., 2009, "Spectral Element Method in Structural Dynamics", John Wiley & Sons, Singapore, 468 p.

Levy, G.N., Schindel, R. and Kruth, J.P., 2003, "Rapid manufacturing and rapid tooling with layer manufacturing (LM) technologies, state of the art and future perspectives", CIRP Annals - Manufacturing Technology, Vol. 52, No. 2, 589-609.

Liu, L. and Hussein, M.I., 2012, "Wave Motion in Periodic Flexural Characterization of the Transition Between Bragg Scattering and Local Resonance", Journal of Applied Mechanics, Vol. 79, pp. 011003-1-17.

Mace, B.R., Duhamel, D., Brennan, M.J. and Hinke, L., 2005 "Finite element prediction of wave motion in structural waveguides", Journal of Acoustic Society of America, Vol. 117, No. 5, pp. 2835-2842.

Pai, P.F., 2010, "Metamaterial-based Broadband Elastic Wave Absorber". Journal of Intelligent Material Systems and Structures, Vol. 21, pp. 517-528.

Pagani, A., Boscolo, M. Banerjee. J.R, and Carrera, E., 2013, "Exact dynamics stiffness elements based on one-dimensional higher-order theories for free vibration analysis of solid and thin-walled structures", Journal of Sound and Vibration, Vol. 332, pp. 6104-6127.

Ruzzene, M., 2015, "Internally Resonating Metamaterials for Wave and Vibration Control", Proceedings of the Noise and Vibration - Emerging Technologies (NOVEM), Dubrovnik, Croatia, pp. FORUMIII3-1-26.

Yao, S., Zhou, X. and Hu,, G., 2008, "Experimental study on negative effective mass in a 1D mass-spring system", New Journal of Physics, Vol. 10, pp. 043020-1-12.

Zhu, R., Huang, G.L., Huang, H.H. and Sun, C.T., 2011, "Experimental and numerical study of guided wave propagation in a thin metamaterial plate". Physics Letters A, Vol. 375, pp. 2863-2867.

RESPONSIBILITY NOTICE

The authors are the only responsible for the material included in this paper.